Ab initio thermodynamics of body-centred cubic and face-centred cubic Cs

2000 J. Phys.: Condens. Matter 12 3293

(http://iopscience.iop.org/0953-8984/12/14/307)

J. Phys.: Condens. Matter **12** (2000) 3293–3312. Printed in the UK PII: S0953-8984(00)10420-5

Ab initio thermodynamics of body-centred cubic and face-centred cubic Cs

N E Christensen†, D J Boers‡, J L van Velsen‡ and D L Novikov§

† Institute of Physics and Astronomy, University of Aarhus, Aarhus C, DK-8000, Denmark
‡ Department of Applied Physics, University of Twente, NL 7500 AE Enschede, The Netherlands
§ Arthur D Little Incorporated, Acorn Park, Cambridge, MA 02140-2390, USA

Received 16 December 1999, in final form 10 February 2000

Abstract. The equation of state of solid caesium (body-centred cubic (bcc) and face-centred cubic (fcc) structures) is examined theoretically by means of *ab initio* calculations. The Helmholtz free energies are calculated for pressures (P) up to 5 GPa and temperatures (T) in the range $0 \rightarrow 300$ K. The electronic contributions are calculated within density-functional theory (local density approximation (LDA) and generalized gradient approximation (GGA)), whereas vibrational contributions to energy and entropy are calculated within the quasi-harmonic approximation. The thermal expansion coefficients (α) of bcc as well as fcc Cs are calculated as functions of P and T. Both phases are predicted to have (P, T) regimes where α is negative. For the fcc phase, α goes negative for P above 3.5 GPa (and up to the end of the stability range of the fcc phase) for *all* T. The value $\alpha = 3.0 \times 10^{-4}$ K^{-1} found for Cs at ambient conditions agrees with experiments, and so does the Debye temperature, 39.5 K. The calculation shows that the bcc $\rightarrow$ fcc transition occurs at $P \approx 2.2$ GPa and low T, and at a higher pressure, $\approx$3 GPa, at room temperature. The fcc phase becomes unstable around 4.3 GPa, where a transverse phonon mode with $\boldsymbol{q}$ along (110) becomes soft. The calculations do not indicate that this transition is isostructural (fcc $\rightarrow$ fcc), a result which is at variance with earlier theoretical and experimental work.

1. Introduction

Caesium undergoes a number of structural phase transitions under pressure. Six phases are known to exist at room temperature: I (bcc), II (fcc), III (collapsed fcc?), IV (tetragonal), V (orthorhombic), and VI (double hexagonal-close-packed) [1–5]. The pressure-driven electronic s $\rightarrow$ d transition in Cs [6] is believed to play a major role in the structural behaviour, at least for pressures up to about 15 GPa corresponding to fourfold compression [7–10]. One of the remarkable features of the structural sequence is the occurrence of the tetragonal phase IV (4.4–12 GPa) which is only eightfold coordinated [2]. The unusual decrease of the coordination number with increasing pressure from 12 in fcc to 8 in Cs-IV has been interpreted in terms of directional bonding induced by the s–d transition [10, 11]. Beyond phase IV the coordination number increases with pressure. The recently determined orthorhombic structure of Cs-V (12 to $\approx$70 GPa) has two non-equivalent crystallographic sites with coordination numbers of 10 and 11 [3], and this *Cmca* structure is the same as that of Si-VI [12, 13].

Cs-III exists only in a narrow pressure range, 4.2 $\rightarrow$ 4.4 GPa, and until recently it was believed to have the fcc structure. The experiments by Hall *et al* [1] indicated that an isostructural fcc $\rightarrow$ fcc transition occurs, and theoretical calculations seemed to confirm this [9, 11]. However, recent experiments [3] have not been able to confirm that Cs-III has the fcc structure. The existence of an isostructural transition would be interesting, in particular

0953-8984/00/143293+20$30.00

because this would imply that the 'normal' metal, Cs, would undergo a transformation similar to the $\alpha \rightarrow \gamma$ transition in Ce, which is due to the 4f electrons (see, for example, reference [14]. and references therein).

Previous calculations [9, 11], as well as the present ones, show that the s $\rightarrow$ d transition in Cs does not produce a van der Waals loop in the pressure–volume relation for fcc Cs obtained from total energies of the electrons alone. But such effects could be caused by the phonons, and therefore their contributions to the free energy must be included. The work in reference [9] used a Debye model for the phonons together with an approximative description of the overall Grüneisen parameter in order to estimate the phonon contribution to the pressure. For certain choices of parameters in the model, a van der Waals loop did occur. However, an evaluation of the rather small phonon contributions requires much better precision. Therefore we calculate full phonon spectra for all relevant volumes, and together with the electronic energies this then leads to free energies as functions of pressure (P), volume (V), and temperature (T). This allows not only a study of the phase transition, but also calculations of thermodynamical quantities, like the thermal expansion coefficient. Further, using the present methods, we can examine the *dynamical* stability of the structure versus P and T. The earlier calculations [9, 11] used electronic total energies obtained within the atomic-spheres approximation (ASA) [15] (with spherical charge distributions inside atomic spheres) which cannot yield energy changes associated with symmetry-breaking distortions. Therefore, such calculations could be used to obtain neither elastic shear constants nor phonon frequencies. This requires methods without shape approximations to potentials and charge densities. Specifically, the ASA calculations would not predict the dynamical instability of fcc Cs as we describe below. Further, the Debye model cannot lead to the peculiar variation of the thermal expansion coefficient with P and T which is predicted here for fcc Cs.

Once we have the free energies on a dense grid in (P, V, T) space it is relatively easy to derive the thermal expansion coefficient as a function of P and T, and this was done for both bcc and fcc Cs. Also the transition pressure of transformation from the bcc to the fcc structure is examined. The equilibrium (i.e. $P = 0$) properties of Cs at room temperature are derived and compared to experiments.

The paper is organized as follows. Our choices of methods for calculation of electronic energies and phonon contributions are described in the next section, section 2. Section 3 presents the results obtained. Subsection 3.1 describes the volume-dependent elastic shear constants, examples of phonon dispersions, and density-of-states functions. The thermodynamical quantities (free energy, entropy, specific heat) and their variation with V are presented in section 3.2, and some of the calculated isotherms are shown in section 3.3 which also contains the thermal expansion coefficients as functions of P and T as well as a discussion of the equilibrium volume of bcc Cs at various temperatures. Conclusions and a summary are given in section 4.

2. Theoretical methods

2.1. Electrons

The total energy of the electrons for a given choice of atomic coordinates (structure and volume) is calculated within approximations to the density-functional theory [18], the local approximation (LDA) as well as a generalized gradient approach (GGA). The majority of the results presented here are obtained with the GGA, and we applied the Perdew–Burke–Ernzerhof scheme [19]. We did, however, choose the parameter κ to be 0.45 (in accordance with previous estimations [20]), i.e. smaller than the 'standard value', 0.806 [19]. The LDA calculations

lead to a non-negligible overbinding in Cs. For example, the theoretical equilibrium volume calculated from the electronic LDA total energies alone is ≈12% smaller than the experimental value at room temperature. Applying the GGA we find that the electronic isotherm has zero pressure for a volume which is 4% smaller than observed. As follows from the results later, the theoretical volume at $T = 300$ K is slightly larger (by ≈2%) than observed.

The solution of the effective one-electron equations was performed by means of the LMTO method [15] in the full-potential version [16,17]. The semi-core states, Cs 5s and 5p, are treated as *local orbitals* [21,22] in the same energy window as the valence states. The bandstructure calculations were scalar relativistic, i.e. all relativistic effects, except spin–orbit splittings, were included. Concerning the bandstructure method, approximations to the exchange and correlation, and basis set, the present calculations are then similar to and consistent with those used earlier [5,13] for the high-pressure phases of Cs.

We have estimated the finite-T contributions to the electronic free energy (energy as well as $-TS$ terms, S being the entropy), and find that they can be neglected in comparison to the phonon terms, except at very special volumes where the phonon contribution to the pressure (nearly) vanishes (sections 3.1 and 3.3).

2.2. Phonons

The phonon contributions to the free energy are calculated within the quasi-harmonic approximation, i.e. the phonon dispersion relations are derived as in usual harmonic approximations, but the force constants (and thus frequencies) vary with volume.

Since we needed to calculate phonon spectra for a large number of volumes, and further needed accurate integrations over the Brillouin zone (BZ), it was necessary that the phonon calculations could be performed quickly and at the same time with good accuracy. We decided to use a method similar to the one suggested by Sharma and Joshi [23], but our final equations and arguments leading to them differ somewhat from theirs.

Within the model, ion–ion interactions are described by interatomic force constants, and the electron gas is assumed to give contributions to the energy stored in the elastic wave through a wavenumber-dependent compressibility term. The energy then becomes [23]

$$\Phi = \Phi_0 + \frac{1}{2}\sum_{m,n}\sum_{i,j}\Phi_{ij}^{mn}u_i^m u_j^n + \frac{1}{2}K_e\Omega\sum_{\boldsymbol{R}}\bar{\chi}^2(\boldsymbol{R}). \tag{1}$$

Here Φ_0 is the equilibrium energy of the crystal, Φ_{ij}^{mn} is the force constant matrix, u_i^m is the ith component of the displacement of the mth ion, K_e is the isothermal compressibility of the conduction-electron gas, Ω is the volume of the primitive unit cell, and $\boldsymbol{R}$ is an equilibrium lattice vector. The average $\bar{\chi}(\boldsymbol{R})$ is defined by

$$\bar{\chi}(\boldsymbol{R}) \equiv \Omega^{-1}\int \chi(\boldsymbol{r})\,\mathrm{d}\boldsymbol{r} \tag{2}$$

where the integral is over the primitive unit cell containing the ion at $\boldsymbol{R}$ and with $\chi(\boldsymbol{r}) = -\boldsymbol{\nabla}\cdot\boldsymbol{u}_e(\boldsymbol{r})$ ($\boldsymbol{u}_e(\boldsymbol{r})$ is the displacement from homogeneity in the electronic medium at the point $\boldsymbol{r}$). The total potential energy stored in the density fluctuations around equilibrium of a homogeneous gas is proportional to $\int \chi^2(\boldsymbol{r})\,\mathrm{d}\boldsymbol{r}$ (where the integral is over all space), and this is approximated by the average equation (1).

With these considerations, the procedure followed by Sharma and Joshi [23] yields the phonon dispersion relations. This involves:

(a) the assumption that the displacement from homogeneity of the electronic medium follows the ionic phonon displacements instantaneously: $\boldsymbol{u}_e(\boldsymbol{r}) = \boldsymbol{e}A\exp(\mathrm{i}\boldsymbol{q}\cdot\boldsymbol{r} - \mathrm{i}\omega t)$;

(b) the approximation of the primitive unit cell with a Wigner–Seitz sphere to accomplish the above indicated spatial averaging;
(c) using the fact that the electron–ion force is proportional to $\nabla\chi(\boldsymbol{r})$; and
(d) using a time average of the potential energy stored in the electronic medium (the third term in equation (1)) to obtain the force constant of the harmonic electron–ion force.

We thus have three equations of the form [24]

$$\lambda\rho\omega^2 = -a^{-3}\sum_n \left\{\lambda\Phi_{11}^{0n} + \mu\Phi_{12}^{0n} + \nu\Phi_{13}^{0n}\right\}\sin^2(\tfrac{1}{2}\boldsymbol{q}\cdot\boldsymbol{R}_n) + V(q) + \sum_{\boldsymbol{K}\neq\boldsymbol{0}}\left\{V\big(|\boldsymbol{q}+\boldsymbol{K}|\big) - V\big(|\boldsymbol{K}|\big)\right\} \tag{3}$$

where

$$V(q) = Lq^2(\lambda L + \mu M + \nu N)\mathcal{G}^2(qr_0)K_{\mathrm{e}}$$

and $\mathcal{G}(x) = (3/x)j_1(x)$ where $j_1(x)$ is the spherical Bessel function of first order. Here, ρ is the mass density of the metal, $\boldsymbol{K}$ denotes a reciprocal-lattice vector, and $2a$ is the lattice parameter. The direction cosines of the polarization vector $\boldsymbol{e}$ and the propagation vector $\boldsymbol{q}$ are denoted by $(\lambda\mu\nu)$ and (LMN), respectively, and the summation over n covers the first- and second-nearest neighbours. Note that the summation over $\boldsymbol{K}$ appearing in equation (3) (which does not appear in references [23, 24]) ensures the proper symmetrization of the dynamical matrix [25]. These terms are important, in particular close to the Brillouin zone boundaries. By taking the long-wavelength limit of equation (3) and comparing the resulting expressions with classical elasticity theory [24], expressions can be found for the Φ_{ij}^{nm} and K_{e} in terms of the elastic constants C_{11}, C_{12}, and C_{44}. We thus obtain the dispersion relation in terms of the elastic constants. These are obtained from total-energy shifts calculated within the density-functional method for the bcc and fcc crystals under deformations. We have used this method to calculate phonon spectra for other bcc and fcc metals (Na, W, Mo, Cu, Ag) [26–29], and found good agreement with experiments (neutron scattering). Figure 1 illustrates this by comparison of calculated and measured [30, 31] phonon frequencies for copper. (Our results differ somewhat from those in figure 1 of reference [24], mainly due to the symmetrizing terms mentioned above.)

From the dispersion relation the phonon density-of-states function, $g(\omega)$, is derived, and from this (here normalized to 3) the basic thermodynamical functions (per atom) are calculated as

$$\begin{aligned} F &= k_B T\int \ln\left\{2\sinh\left(\frac{\hbar\omega}{2k_BT}\right)\right\}g(\omega)\,\mathrm{d}\omega \\ E &= \frac{1}{2}\hbar\int \coth\left(\frac{\hbar\omega}{2k_BT}\right)\omega g(\omega)\,\mathrm{d}\omega \\ S &= k_B\int\left\{\frac{\hbar\omega}{2k_BT}\coth\left(\frac{\hbar\omega}{2k_BT}\right) - \ln\left[2\sinh\left(\frac{\hbar\omega}{2k_BT}\right)\right]\right\}g(\omega)\,\mathrm{d}\omega \end{aligned} \tag{4}$$

where F, E, and S denote the Helmholtz free energy, the energy, and the entropy, respectively. The phonon contribution to the specific heat is

$$C_V = nk_B\int\left(\frac{\hbar\omega}{2k_BT}\right)^2\mathrm{cosech}^2\left(\frac{\hbar\omega}{2k_BT}\right)g(\omega)\,\mathrm{d}\omega \tag{5}$$

where n is the concentration of atoms. When the volume dependence of the elastic constants is known, so is that of $g(\omega)$ and we have the thermodynamic quantities pertaining to the phonons as functions of temperature and volume. It should be noted, however, that the elastic constants are in general also dependent on temperature. The variation of the shear constants with T has been examined experimentally in reference [32].

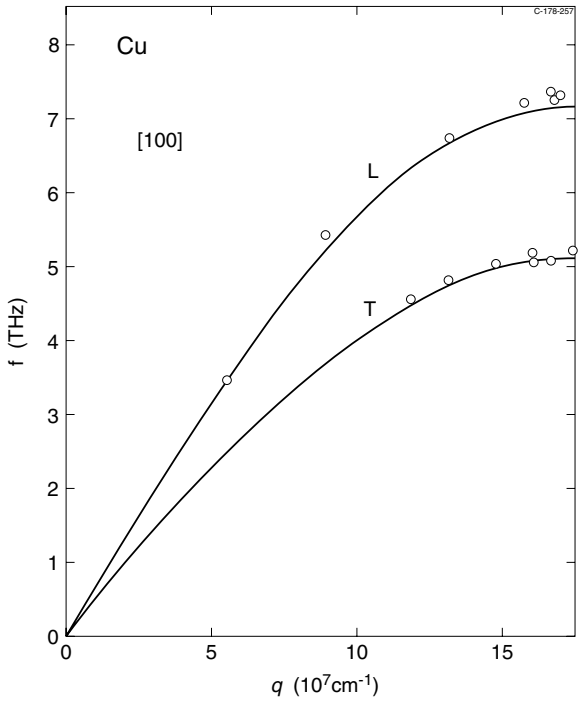

Figure 1. Phonon dispersion curves calculated for copper along (100) by means of the method described here (full lines), and experimental results given by Cribier *et al* (reference [30] and reference [31]).

3. Results

This section is divided into three subsections, the first one describing the calculation of elastic constants and phonon dispersion relations and density-of-states functions. The next section summarizes the calculations of the thermodynamic functions, energy, free energy, etc versus V and T. Also the bcc $\rightarrow$ fcc transition pressure is calculated. The last subsection presents the thermal expansion coefficients, and we show that bcc as well as fcc Cs have regimes with negative expansion coefficients.

3.1. Elastic constants and phonons

The practical calculations of the elastic constants for Cs turned out to be much more time consuming than for, for example, Mo and W. The reason is that Cs is extremely soft, and therefore the energy changes caused by the shear deformations are very small, in some cases of the order of 10 μRyd or less. The electronic bandstructures had to be calculated over many k-points, more than 14 000 in the irreducible BZ, in order to obtain results with sufficiently small numerical scatter. The calculations presented here were all performed within the GGA. But we did also calculate all elastic constants with the LDA, and it was found that C_{44} and C' at all volumes were extremely close to the values obtained using the GGA, in spite of the overbinding mentioned in section 3.1.

Applying volume-conserving strains in the (001) and (111) directions then allowed calculation of the tetragonal, $C' = \frac{1}{2}(C_{11} - C_{12})$, and trigonal, C_{44}, shear constants. For

several volumes the total energy was calculated for five tetragonal and five trigonal volume-conserving distortions. Polynomial least-squares fits of the energy versus strain parameter then allowed derivation of the tetragonal- and trigonal-shear constants as functions of volume. The ground-state pressure–volume relation was obtained from the volume derivative of the total-energy–volume curve which was obtained by fitting a suitable series of functions to the energies obtained for the undistorted crystal.

(By a 'suitable series' we mean a power series in $X = (V/V_0)^{1/3}$, including positive and negative powers. The fit was made to 27 to 30 primary calculations, and this means that the energy span to be fitted is of the order of 60 mRyd/atom, only. Since the energy *changes* are converged with respect to basis set, k-integration etc to 1 μRyd or better, high-quality fits are obtained. $P(V)$ and $B(V)$ are obtained from analytic expressions once the coefficients in the E–V fit are known.)

This also yielded the bulk modulus B as a function of volume, and this then allowed the calculation of the separate shear constants C_{11} and C_{12} from the relation

$$B = (C_{11} + 2C_{12})/3. \tag{6}$$

In the following, V_0 denotes the experimental equilibrium volume of Cs (bcc) at room temperature. We use $V_0 = 747.236$ Bohr^3/atom (corresponding to the bcc lattice parameter $a_{bcc} = 6.05$ Å). Figure 2 shows the calculated elastic constants for fcc Cs, whereas those obtained for the bcc phase are given in figure 3. Already these results show that instabilities occur as the lattices are compressed. As V/V_0 is reduced below 0.45, C' for the fcc phase drops rapidly and becomes negative. Below $V \approx 0.43V_0$, the fcc lattice is no longer dynamically stable. Something similar happens to C' for the bcc structure as V/V_0 is made smaller than $\approx$0.6. This is the regime where the bcc $\rightarrow$ fcc transition occurs.

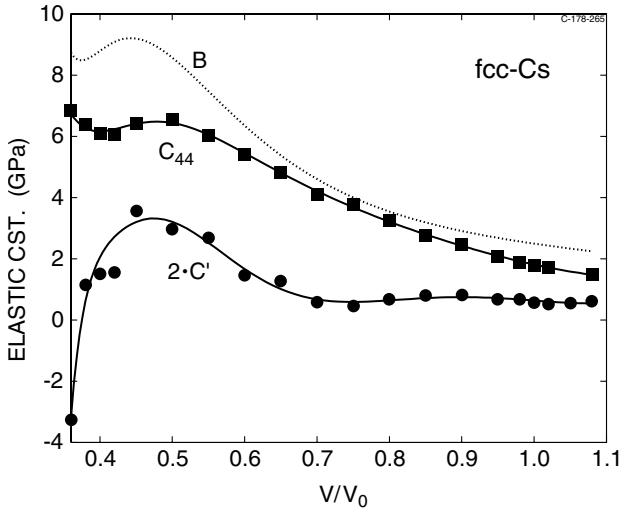

Figure 2. The elastic constants for the fcc phase. Full lines are polynomial fits. The dotted curve is the bulk modulus, squares denote the calculated points for C_{44} while those for $2C' = C_{11} - C_{12}$ are denoted by circles.

As mentioned earlier, Cs is very soft. This is reflected in the very small values of C': some are below 0.5 GPa. This also means that the data show some numerical scatter, although many k-points were used. The phonon dispersion relations and density-of-states (DOS) functions were calculated for a large number of volumes. Figure 4 shows three examples of the dispersion

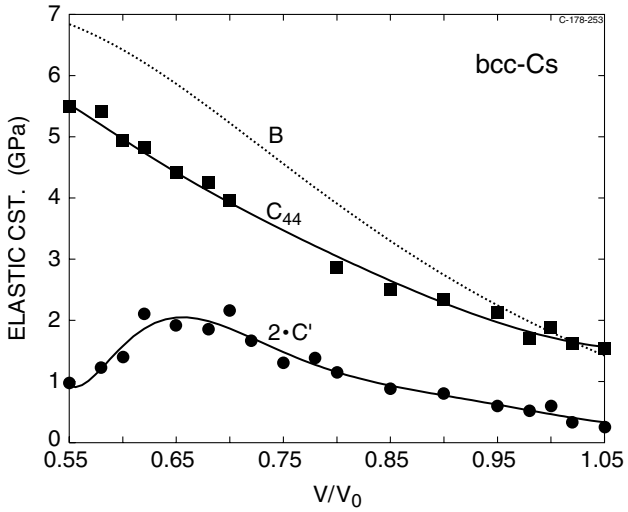

Figure 3. The elastic constants for the bcc phase. Full lines are polynomial fits. The symbols are as in figure 2.

relations obtained for fcc Cs. It is seen that a compression of the lattice from $V/V_0 = 0.80$ (dash–dotted lines) to $V/V_0 = 0.50$ (full lines) leads to an increase of the frequencies in all modes. This is the 'normal' behaviour, since usually a crystal hardens under compression. Also, figure 2 shows that all elastic constants at $V/V_0 = 0.80$ are smaller than those at $V/V_0 = 0.50$. Upon further compression the situation becomes quite different. The tetragonal-shear constant C' decreases rapidly (figure 2), and the crystal becomes softer. The dotted curves in figure 4 show that at $V/V_0 = 0.376$ all frequencies are *lower* than those found for $V/V_0 = 0.50$ (full lines). In addition we find that one mode, the lowest transverse mode with wave vector $\boldsymbol{q}$ along (110), becomes soft in the long-wavelength limit. At $V/V_0 = 0.376$ it

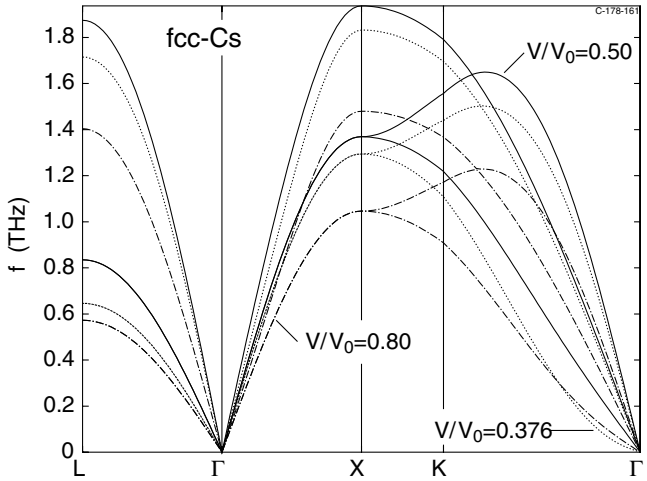

Figure 4. Phonon dispersion relations for fcc Cs for the volumes $V/V_0 = 0.376$ (dotted curves), $V/V_0 = 0.50$ (full lines), $V/V_0 = 0.80$ (dash–dotted curves).

already drops below the corresponding curve for $V/V_0 = 0.80$, and further compression would (formally) lead to imaginary frequencies. This is the volume range where the fcc structure of Cs becomes unstable, and it transforms to Cs-III and then on to Cs-IV etc. The softening of fcc Cs under compression is also illustrated in figure 5, which shows the phonon DOS for the three volumes selected for figure 4. Figure 6 shows examples of phonon DOS for bcc Cs.

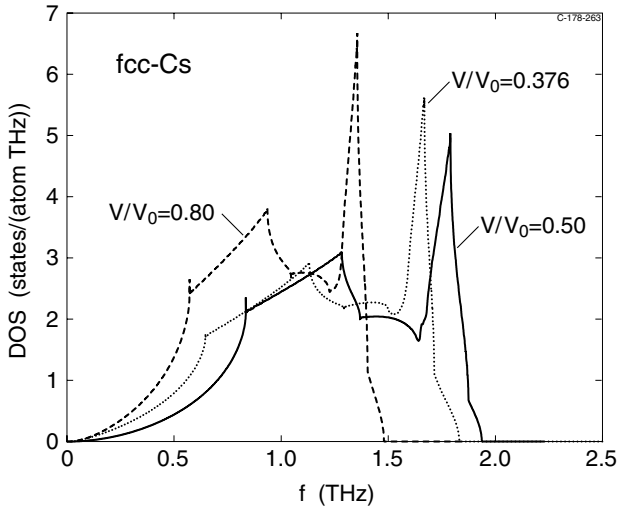

Figure 5. The phonon density-of-states function at $V/V_0 = 0.376$ (dotted), $V/V_0 = 0.50$ (full line), and $V/V_0 = 0.80$ (dashed) for fcc Cs. The density-of-states function is normalized to 3.

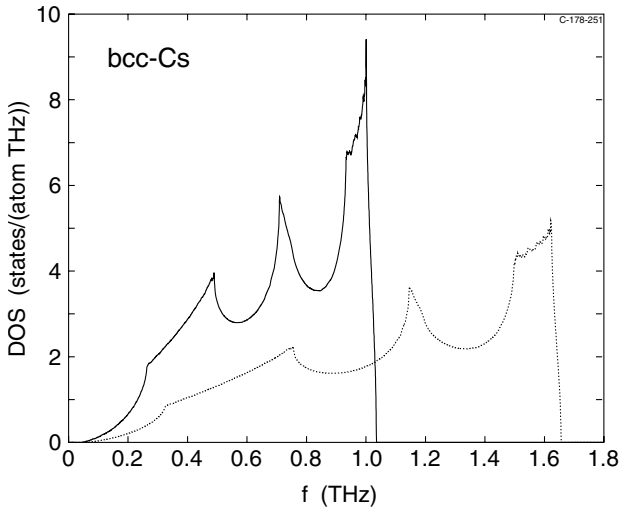

Figure 6. The phonon density-of-states function at $V/V_0 = 0.55$ (dotted curve) and $V/V_0 = 1.00$ for the bcc phase. The density-of-states function is normalized to 3.

Phonon frequencies as calculated by the method described here are for bcc Cs at $V/V_0 = 1.00$ compared to other theoretical results [33–35] and to experiments [36, 37] in table 1. Only two symmetry points are included in table 1, but these are representative of the

Table 1. Theoretical and experimental phonon frequencies (in 10^{12} Hz) for bcc Cs, $V/V_0 = 1.0$, at the symmetry points H (100) and N (110) for longitudinal (L) and transverse (T) modes.

	L(H)	L(N)	T(N)	T(N)
Theory[a]	1.03	1.20	0.24	0.71
Theory[b]	1.09	1.29	0.21	0.70
Theory[c]	1.06	1.20	0.23	0.72
Present	0.98	1.03	0.29	0.69
Experiment[d]	0.96	1.07	0.22	0.63
Experiment[e]	0.90	1.07	0.22	0.58

[a] Pseudopotential calculation, Taylor and MacDonald [33].
[b] Pseudopotential calculation, Moriarty [34].
[c] Pseudopotential calculation, Chung *et al* [35].
[d] Inelastic neutron scattering, Nücker and Buchenau [36], on polycrystalline Cs at 50 K.
[e] Inelastic neutron scattering, Mizuki and Stassis [37], on single crystals.

level of overall agreement. The elastic constants, also for bcc Cs at the equilibrium volume, are in table 2 compared to values deduced from the neutron scattering data [37] and from sound speed experiments by Kollarits and Trivisonno [32].

Table 2. Experimental elastic constants of bcc Cs at the equilibrium volume as obtained experimentally and as calculated in the present work. The units are GPa (or 10^{10} dyn cm^{-2}).

	C_{11}	C_{12}	C_{44}
Present	2.10	1.50	1.56
Experiment[a]	2.47	2.06	1.48
Experiment[b]	1.60	0.99	1.44

[a] Sound velocity measurement at $T = 78$ K, Kollarits and Trivisonno [32].
[b] Inelastic neutron scattering, Mizuki and Stassis [37].

3.2. Thermodynamical functions

This section summarizes our calculations of the phonon contributions to the energy (E), Helmholtz free energy ($F = E - TS$), entropy (S), and their variations with T and V. Also the phonon contribution to $C_V(T)$ is presented, and in addition we discuss the fcc–bcc structural difference in Gibbs free energy, including contributions from the phonons as well as from the electrons. This allows a theoretical estimate of the bcc $\rightarrow$ fcc transition pressure (or, rather, the fcc–bcc *coexistence pressure*).

Figures 7, 8, and 9 show, for bcc Cs, E and F versus T for a specific volume, and S and F versus V for three selected temperatures, and figures 10, 11, and 12 are similar plots for the fcc phase. Figure 12 shows that F is maximum at $V/V_0 \approx 0.50$, and in fact it was found that this maximum occurs at the same volume irrespective of the temperature. A similar observation was not made for bcc Cs.

The calculated phonon specific heats and entropies versus T for fixed volumes are shown in figures 13 and 14. The Dulong–Petit value of C_V is $3nk_B$. The Debye temperature, Θ_D, can be extracted from the phonon contribution to the specific heat at low temperatures:

$$C_V = \frac{12\pi^4}{5} nk_B \left(\frac{T}{\Theta_D} \right)^3. \tag{7}$$

Figure 15 shows the resulting Θ_D versus V for fcc and bcc Cs. For $V/V_0 = 1.00$ we obtain for the bcc phase $\Theta_D = 39.5$ K. This agrees very well with the value, 39 K, obtained

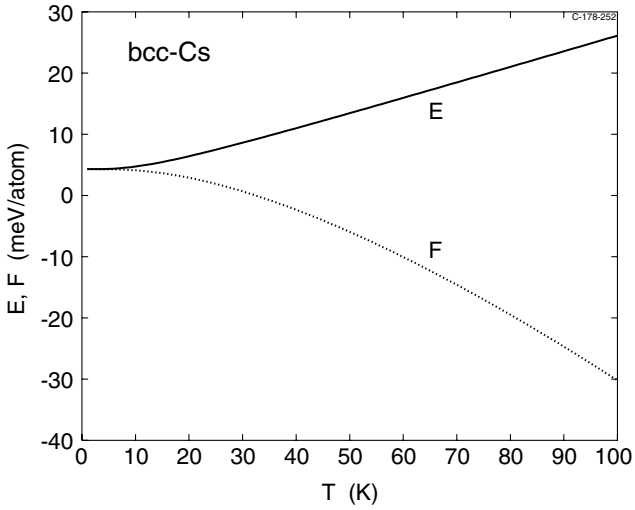

Figure 7. The phonon energy and free energy (dotted curve) at $V/V_0 = 1.00$, for the bcc phase.

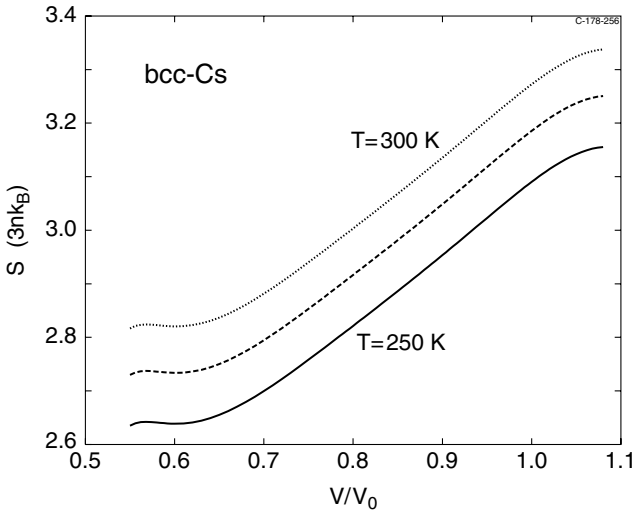

Figure 8. The phonon entropy at $T = 250$ K (full line), $T = 275$ K (dashed line), and $T = 300$ K (dotted line), for the bcc phase.

from the calorimetric data by Filby and Martin [38]. We also show, figure 16, the zero-point energy as well as the same quantities calculated within the Debye model:

$$E_{zp} = \frac{9}{8} k_B \Theta_D. \tag{8}$$

As expected, this frequently used approximation yields relatively good estimates for both phases.

A review of specific heat data for the alkali metals was given by Martin [39] who mentions that it appears [40] that the analysis of calorimetric data, at least at high temperatures, is best made in terms of the entropy rather than the specific heat. Reference [39] contains tabulations of entropy versus temperature, and in figure 17 these data are shown (dots) together with our

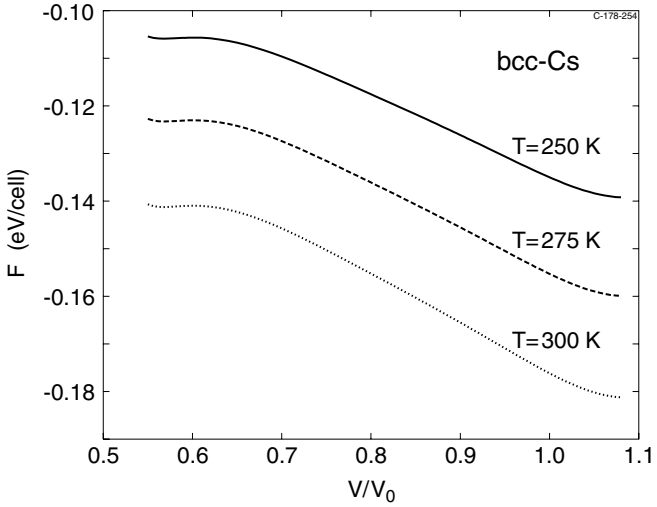

Figure 9. The phonon free energy at $T = 250$ K (full line), $T = 275$ K (dashed line), and $T = 300$ K (dotted line), for the bcc phase.

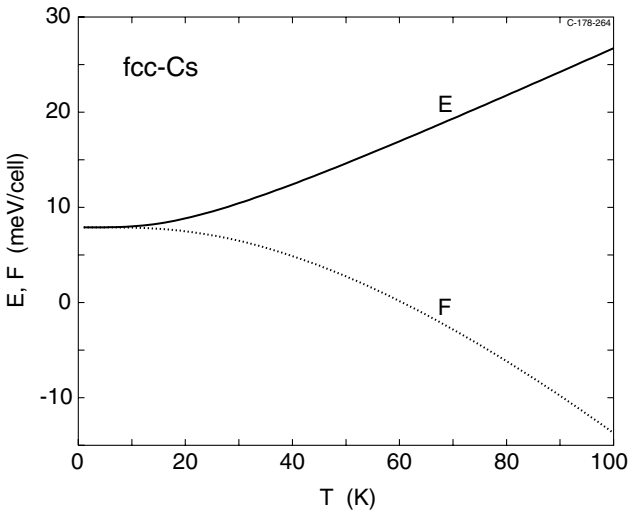

Figure 10. The phonon free energy (dotted curve) and energy (full line) at $V/V_0 = 0.50$, for the fcc phase.

calculations (bcc Cs at $V/V_0 = 1.00$) (full line). Although theory and experiment appear to agree rather well, a deviation that increases with temperature can clearly be seen. The calculation is strictly harmonic. According to Tosi and Fumi [40] the leading anharmonic contribution to the entropy is given by

$$S - S_{harm} = 3nk_B AT. \tag{9}$$

The dashed curve in figure 17 is obtained by adding to our calculated $S(T)$ such a term with $A = 2.9 \times 10^{-4}$. This modified $S(T)$ is now very close to the experimental results. Martin made a similar analysis, assuming that the C_V-data below a certain temperature, T', are purely harmonic, and found $A = (2.3 \pm 0.1) \times 10^{-4}$, however with the reservation that the

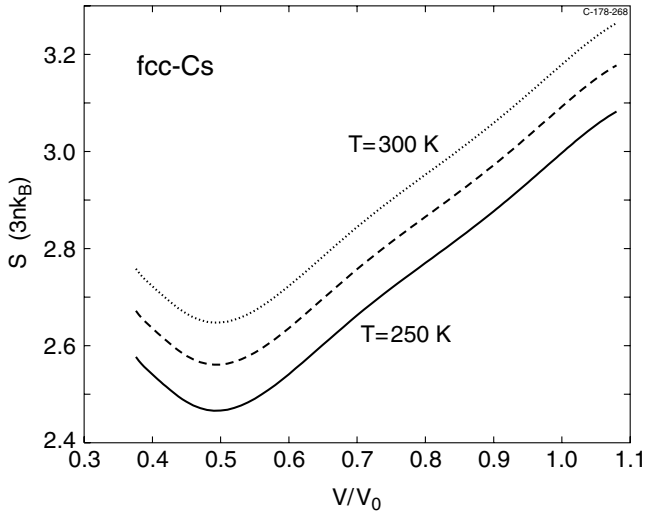

Figure 11. The phonon entropy at $T = 250$ K (full line), $T = 275$ K (dashed line), and $T = 300$ K (dotted line), for the fcc phase.

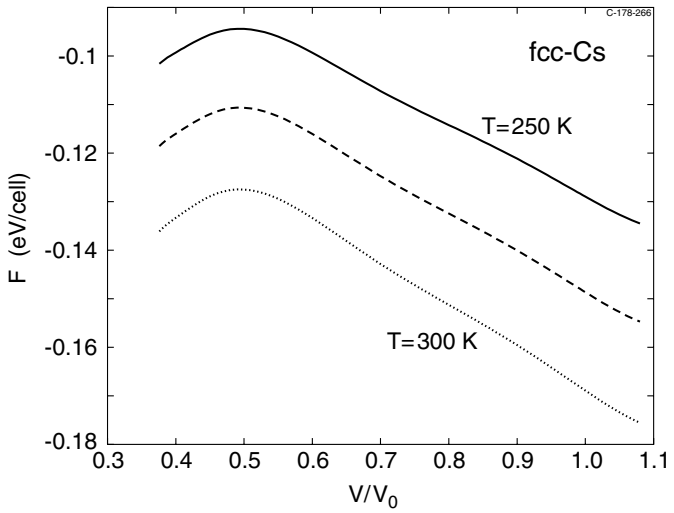

Figure 12. The phonon free energy at $T = 250$ K (full line), $T = 275$ K (dashed line), and $T = 300$ K (dotted line), for the fcc phase.

size of the error bar depends on the validity of the chosen T', for Cs taken to be 70 K.

Having calculated $F(V)$ for various temperatures, T, we derived $P(V, T)$, and then the Gibbs free energy, $G = F + PV$. By comparing $G(P, T)$ for bcc and fcc Cs we can determine the relative stability of these two phases at a given pressure and a certain temperature. Figure 18 shows the calculated structural difference

$$\Delta G(P, T) = G_{bcc}(P, T) - G_{fcc}(P, T)$$

as a function of P for $T = 0$ and 200 K. The calculations predict that at $T = 0$, the bcc phase should be more stable than the fcc phase for P below 2.2 GPa (P_t(bcc $\rightarrow$ fcc)). Calculations for finite values of T show that P_t increases with temperature. Figure 18 shows that $P_t \approx 2.6$ GPa

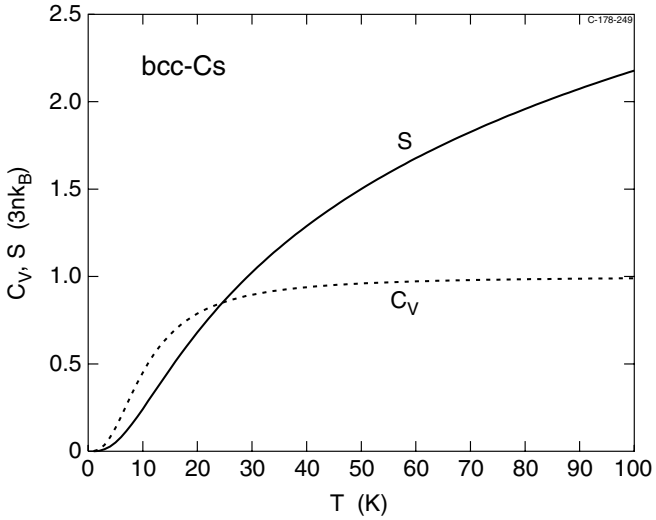

Figure 13. The phonon specific heat (dotted curve) and entropy at $V/V_0 = 1.00$, for the bcc phase.

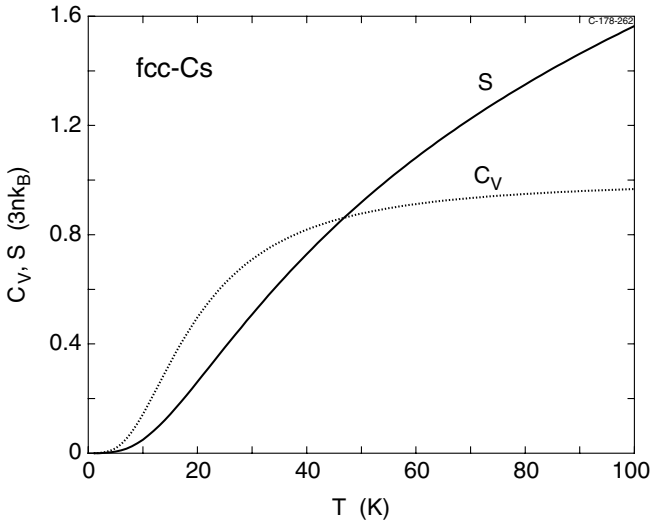

Figure 14. The phonon specific heat (dotted curve) and entropy (full line) at $V/V_0 = 0.50$, for the fcc phase.

at $T = 200$ K, and it further increases to ≈3 GPa at 300 K. (The error bars are rather large at high T because the F-values for the bcc phase have large errors close to the instability of this phase.) Experimentally, the bcc → fcc transition was observed [1] to take place at 2.3 GPa. In view of the very small energy differences, figure 18, it is concluded that theory and experiment agree extremely well. Further, figure 18 shows that, at low pressures, an increase in temperature tends to stabilize further the bcc phase over the fcc phase. At T close to 0, only a small hypothetical volume *expansion* would be needed to make fcc Cs energetically more favourable.

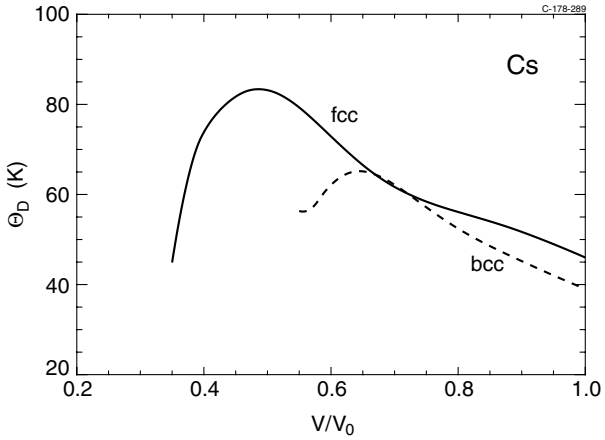

Figure 15. Debye temperatures of fcc and bcc Cs as calculated as functions of volume.

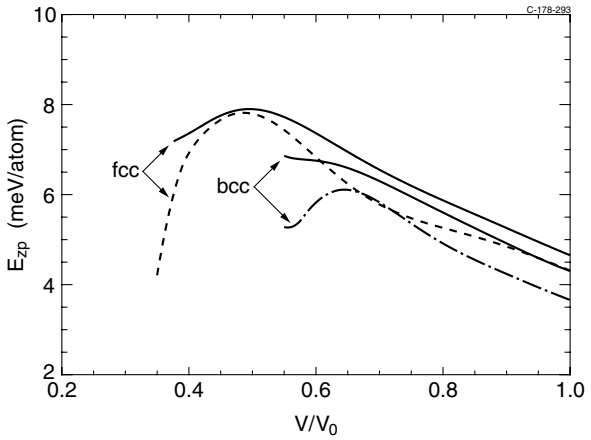

Figure 16. The energy associated with the zero-point motion as obtained directly (full lines) from the common $T \rightarrow 0$ limit of the phonon energies E and F. The dashed and dash–dotted lines show the zero-point energy as obtained from the Debye model.

3.3. Thermal expansion coefficients and isotherms

The thermal (volume) expansion coefficient

$$\alpha = [\mathrm{d} \ln V / \mathrm{d}T]_P \tag{10}$$

was calculated for bcc as well as fcc Cs as functions of both P and T. First, we consider bcc Cs, and figure 19 shows the calculated α for $T = 290$ K versus P in the low-pressure regime. It is noted that for $P \rightarrow 0$, α tends towards 3.0×10^{-4} K^{-1}. This agrees with the experimental value quoted in standard tables, for example reference [41]: $\alpha = 2.91 \times 10^{-4}$ K^{-4}.

The thermal expansion coefficient of Cs decreases if, at a fixed temperature, the pressure is increased. The calculations, figure 20, show this in the low-temperature regime for pressures varying over the range where the bcc structure is dynamically stable. For the temperatures represented in figure 20 the calculations predict that α is negative for pressures above $\approx$2 GPa. We have neglected the electronic contributions to α, but these are estimated to be smaller than 10^{-7} K^{-1} at $T = 10$ K, and this is not sufficient to make all the α-values positive. It should be

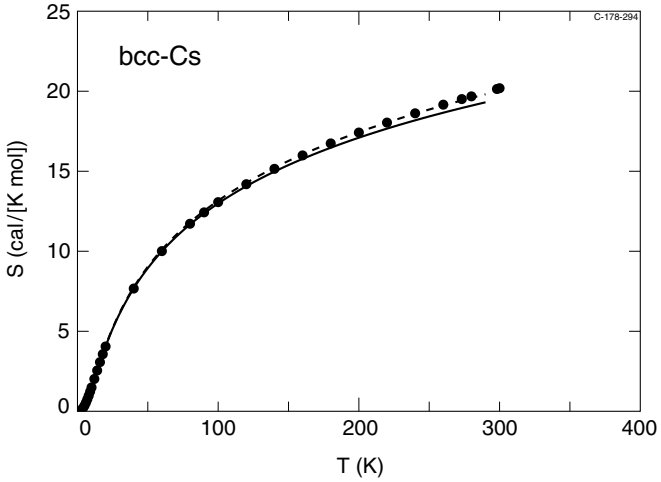

Figure 17. The entropy calculated for bcc Cs at the equilibrium volume versus temperature (full line) and the data derived [39] from experiments (filled circles). The dashed line represents the calculations after addition of a correction for anharmonic effects.

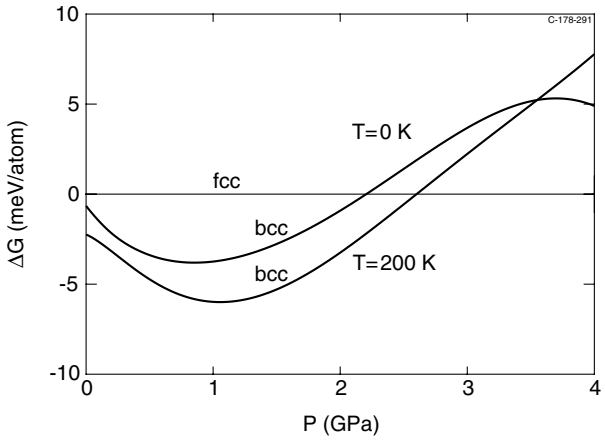

Figure 18. The structural difference in Gibbs free energy, $\Delta G = G_{bcc} - G_{fcc}$ as a function of P for $T = 0$ and 200 K.

noted, however, that there are cases where the electronic contributions to the thermal expansion coefficients become important. Typically, this happens when a Van Hove singularity is close to the Fermi level and thus can contribute significantly to the derivative of the density of states with respect to structural parameters (volume, for example). Examples of this are discussed in references [42–44].

The temperature dependence of α for bcc Cs for fixed pressures is illustrated in figure 21. For $P = 0$ one recognizes the qualitative T-dependence found for C_V, figure 13. The lowest curve ($P = 2.2$ GPa) illustrates again the negative expansion coefficient close to the bcc $\rightarrow$ fcc transition. The calculated $C_V(T)$ for compressed volumes resemble very much those calculated at equilibrium. Thus, the approximate relation

$$\alpha = \frac{\gamma C_V}{B} \tag{11}$$

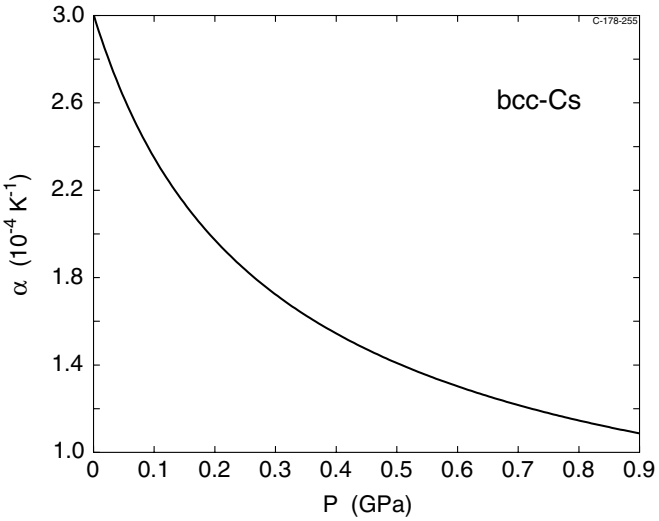

Figure 19. The thermal expansion of the bcc phase at $T = 290$ K. The zero-pressure value is 3.0×10^{-4} K^{-1}.

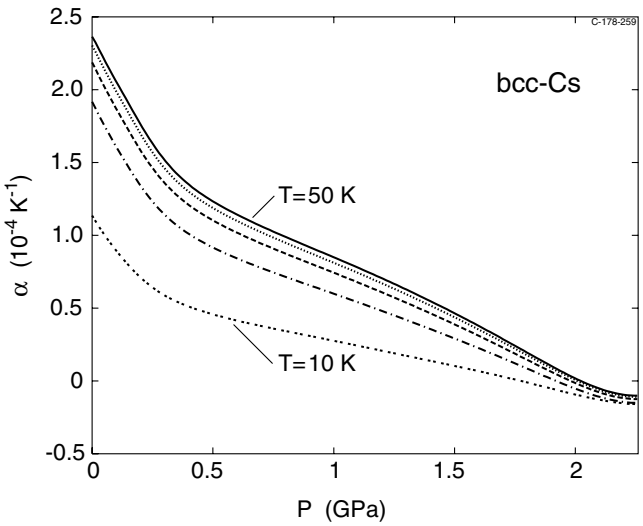

Figure 20. The thermal expansion coefficient versus P for bcc Cs for the temperatures 10, 20, 30, 40, and 50 K.

requires the *overall Grüneisen parameter* γ to be negative in that pressure range. Also the fcc phase of Cs is found to have a regime where the thermal expansion coefficient is negative. Figure 22 shows that for fcc Cs, α goes through zero at a single value of P (3.5 GPa) *irrespective* of the temperature. This is a consequence of all mode-Grüneisen parameters vanishing at a specific volume as mentioned earlier. At this volume, therefore, the phonon contributions to the pressure disappear (cf. also the discussion of $F(V)$ earlier). It could be argued that we in this regime should include the electronic finite-T contributions, but they would only introduce small shifts of the crossover point.

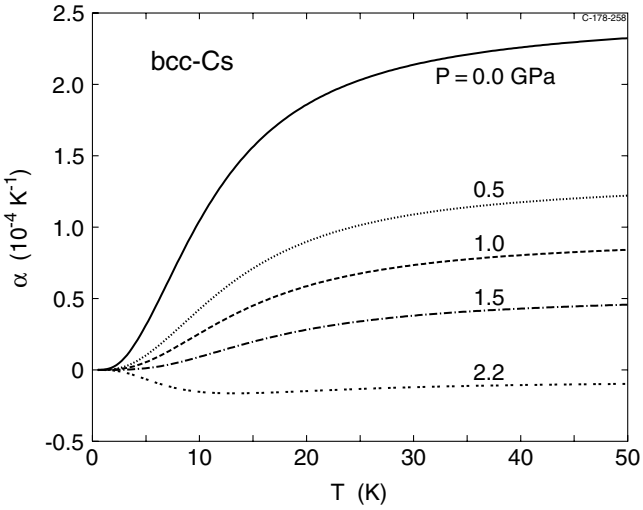

Figure 21. The thermal expansion coefficient, α, of bcc Cs at the pressures 0.0, 0.5, 1.0, 1.5, and 2.2 GPa.

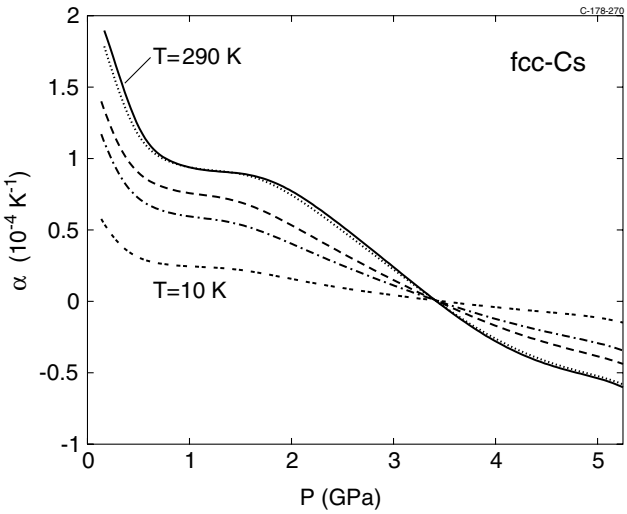

Figure 22. The thermal expansion coefficient of the fcc phase for the temperatures 10, 20, 30, 200, and 290 K.

The disappearance of the phonon contribution to the pressure is also evident from the calculated isotherms, figure 23. These, as well as any other isotherms which we calculated for fcc Cs, do not exhibit a van der Waals loop even down to $V/V_0 = 0.37$. We do find that the phonons cause a softening of the lattice leading finally to thermodynamical instability, but we do not find a first-order fcc $\rightarrow$ fcc transition.

We are now able to examine the theoretical equilibrium volume of bcc Cs. In figure 24 the low-pressure parts of five calculated isotherms are shown. As mentioned earlier, the $T = 0$ isotherm crosses $P = 0$ at $V/V_0 = 0.96$, V_0 being the observed volume at ambient conditions. This does not indicate an overbinding in the GGA calculation. Rather the theoretical volumes are slightly too large: at $T = 300$ K the calculated volume is $\approx 2\%$ larger than V_0. This

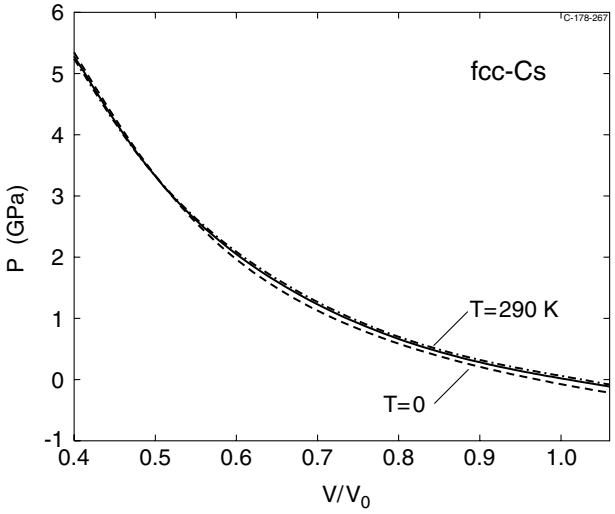

Figure 23. Isotherms for the fcc phase for the temperatures 0, 200, and 290 K.

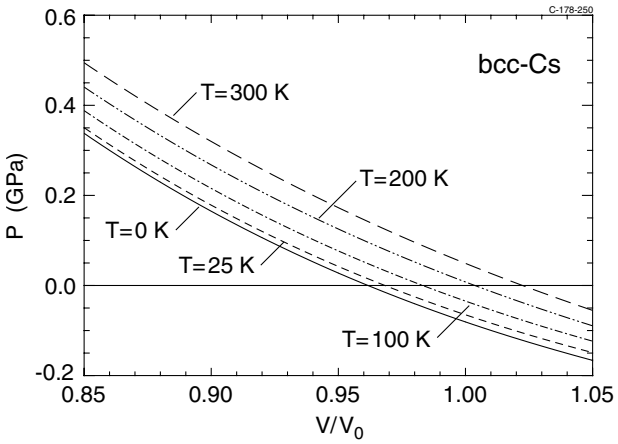

Figure 24. Isotherms for the bcc phase for the temperatures 0, 25, 100, 200, and 300 K. The 300 K isotherm crosses zero at $V/V_0 = 1.02$. (The isotherm for $T = 0$ shown here was calculated without zero-point motion.)

result, together with the value of α calculated for bcc Cs at ambient conditions, indicates close agreement with experiments.

4. Conclusions

Solids with negative thermal expansion coefficients are not unknown. Diamond- and zinc-blend-type semiconductors exhibit negative α at about 100 K; see, for example, reference [45] and the theoretical analysis by Biernacki and Scheffler [46]. The behaviour found here for Cs, in particular fcc Cs, is different because α is predicted to be negative at *all* temperatures for pressures above 3.5 GPa and up to the pressure at which the fcc structure is dynamically unstable (around 4.3 GPa). As a consequence of this instability, the isostructural fcc $\rightarrow$ fcc

transition cannot occur in Cs. Thus, Cs-III must have a structure different from fcc.

Concerning the electron contributions it has been shown that the usual LDA leads to a rather large overbinding in Cs. The GGA, with reduced κ in the PBE version, yields, when thermal expansion is properly taken into account, an equilibrium volume in good agreement with experiment. LDA and GGA yield very similar results for the elastic constants versus volume.

It is particularly important to include the thermal effects when comparing to room-temperature experiments in the case of Cs, because these effects are very large for this metal. At ambient conditions Cs has a (volume) thermal expansion coefficient which is $3.0 \times 10^{-4}\ \mathrm{K}^{-1}$. This is $\approx$7 times that of silver. The value cited here for Cs is obtained in the present calculation, and it agrees with experiment. Also the theoretical value, 39.5 K, of the Debye temperature of caesium at ambient conditions is close to experimental results, 38 and 40 K.

The calculated Gibbs free energy of bcc Cs is lower than that of the fcc phase for $P < P_t$, where $P_t \approx 2.2$ GPa at $T = 0$, and increasing with temperature: $P_t \approx 3$ GPa at room temperature. In view of the small bcc–fcc structural energy differences, $\approx$0.5 mRyd/atom, the agreement with experiment, $P_t = 2.3$ GPa, is excellent.

References

[1] Hall H T, Merrill L and Barnett J D 1964 *Science* **146** 1297
[2] Takemura K, Minomura S and Shimomura O 1982 *Phys. Rev. Lett.* **49** 1772
[3] Schwarz U, Takemura K, Hanfland M and Syassen K 1998 *Phys. Rev. Lett.* **81** 2711
[4] Takemura K, Shimomura O and Fujihisa H 1991 *Phys. Rev. Lett.* **66** 2014
[5] Takemura K, Christensen N E, Novikov D L, Syassen K, Schwarz U and Hanfland M 2000 *Phys. Rev.* B submitted
[6] Sternheimer R 1950 *Phys. Rev.* **78** 235
[7] Louie S G and Cohen M L 1974 *Phys. Rev.* B **10** 3237
[8] McMahan A K 1978 *Phys. Rev.* B **17** 1521
[9] Glötzel D and McMahan A K 1979 *Phys. Rev.* B **20** 3210
[10] McMahan A K 1984 *Phys. Rev.* B **29** 5982
[11] Christensen N E, Pawlowska Z and Andersen O K 1986 unpublished
[12] Hanfland M, Schwarz U, Syassen K and Takemura K 1999 *Phys. Rev. Lett.* **82** 1197
[13] Christensen N E, Novikov D L and Methfessel M 1999 *Solid State Commun.* **110** 615
[14] Liu L Z, Allen J W, Gunnarsson O, Christensen N E and Andersen O K 1992 *Phys. Rev.* B **45** 8934
[15] Andersen O K 1975 *Phys. Rev.* B **12** 3060
[16] Methfessel M 1988 *Phys. Rev.* B **38** 1537
[17] Methfessel M and van Schilfgaarde M, unpublished
[18] Hohenberg P and Kohn W 1964 *Phys. Rev.* **136** B864
Kohn W and Sham L J 1965 *Phys. Rev.* **140** A113
Sham L J and Kohn W 1966 *Phys. Rev.* **145** 561
[19] Perdew J P, Burke K and Ernzerhof M 1996 *Phys. Rev. Lett.* **77** 3865
[20] Peltzer y Blancá E L, Rodriguez C O, Shitu J and Novikov D L, unpublished
[21] Singh D J 1994 *Planewaves, Pseudopotentials and the LAPW Method* (Boston, MA: Kluwer Academic)
[22] van Schilfgaarde M, unpublished
[23] Sharma P K and Joshi S K 1963 *J. Chem. Phys.* **39** 2633
[24] Sharma P K and Joshi S K 1964 *J. Chem. Phys.* **40** 662
[25] See, for example, Problem 26.1 in Ashcroft N W and Mermin N D 1976 *Solid State Physics* (Philadelphia, PA: Saunders College)
[26] Christensen N E and Seraphin B O 1971 *Phys. Rev.* B **4** 3321
[27] Christensen N E 1993 unpublished
[28] Christensen N E, Ruoff A L and Rodriguez C O 1995 *Phys. Rev.* B **52** 9121
[29] Ruoff A L, Rodriguez C O and Christensen N E 1998 *Phys. Rev.* B **58** 2998
[30] Cribier D, Jacrot B and Saint-James D 1960 *J. Physique Radium* **21** 67
[31] Cribier D, Jacrot B and Saint-James D 1961 *Proc. Symp. on Inelastic Scattering of Neutrons in Solids and Liquids* (Vienna: International Atomic Energy Agency) p 549
[32] Kollarits F J and Trivisonno J 1968 *J. Phys. Chem. Solids* **29** 2133

[33] Taylor R and MacDonald A H 1980 *J. Phys. F: Met. Phys.* **10** 2387
[34] Moriarty J A 1974 *Phys. Rev.* B **10** 3075
[35] Chung M S, Cutler P H and Sun F 1986 *Phys. Rev.* B **33** 2125
[36] Nücker N and Buchenau U 1985 *Phys. Rev.* B **31** 5479
[37] Mizuki J and Stassis C 1986 *Phys. Rev.* B **34** 5890
[38] Filby J D and Martin D L 1965 *Proc. R. Soc.* **284** 83
[39] Martin D L 1965 *Phys. Rev.* **139** A150
[40] Tosi M P and Fumi F G 1963 *Phys. Rev.* **131** 1458
[41] Grey D E (ed) 1957 *American Institute of Physics Handbook* (New York: McGraw-Hill) table 4f-3, pp 4–56
[42] Antropov V, Katsnelson M I, Koreshkov V G, Likhtenstein A I, Trefilov A V and Vaks V G 1988 *Phys. Lett.* A **130** 155
[43] Nizhankovski V I, Katsnelson M I, Peschanskikh G V and Trefilov A V 1994 *Pis. Zh. Eksp. Teor. Fiz.* **59** 693 (Engl. Transl. 1994 *JETP Lett.* **59** 733)
[44] Novikov D L, Katsnelson M I, Trefilov A V, Freeman A J, Christensen N E, Svane A and Rodriguez C O 1999 *Phys. Rev.* B **59** 4557
[45] Dolling G and Cowley R A 1966 *Proc. Phys. Soc.* **88** 463
[46] Biernacki S and Scheffler M 1989 *Phys. Rev. Lett.* **63** 290